

# Understanding the relativistic overdensity of galaxy surveys

**Didam G.A. Duniya**

<sup>1</sup>Department of Mathematics & Applied Mathematics, University of Cape Town, Cape Town 7701, South Africa

<sup>2</sup>African Institute for Mathematical Sciences (AIMS), Cape Town 7945, South Africa

<sup>3</sup>Department of Physics & Astronomy, University of the Western Cape, Cape Town 7535, South Africa

<sup>4</sup>Department of Physics & Astronomy, Botswana International University of Science and Technology, Palapye, Botswana

E-mail: [adamsgwazah@gmail.com](mailto:adamsgwazah@gmail.com)

**Abstract.** The main goal of galaxy surveys is to map the distribution of the galaxies, for the purpose of understanding the properties of this distribution and its implications for the content and evolution of the universe. However, in order to realise the potential of these surveys, we need to ensure that we are using the correct analysis: the relativistic analysis, which has been widely studied recently. In this work, the known relativistic overdensity of galaxy surveys is re-examined. Subtle, yet crucial parameters which appear to have been missed by previous works are uncovered. The possible implication of these parameters on the observed galaxy power spectrum is demonstrated for a generic survey, in the cosmological concordance model. The results show that these parameters can alter the predictions of galaxy clustering on all scales; hence, the relativistic effects (on ultra-large scales). In particular, the results show that ignoring these parameters—as in the analysis in previous works—will lead to a false overestimation of the galaxy clustering strength in structure formation.

**Keywords:** Dark energy, modified gravity, galaxy clustering, large scales, power spectrum, relativistic corrections

---

## Contents

<b>1</b>	<b>Introduction</b>	<b>1</b>
<b>2</b>	<b>The Relativistic Galaxy Overdensity</b>	<b>2</b>
2.1	The Cumulative Number Densities	2
2.2	The Galaxy Number per Unit Solid Angle per Redshift	3
2.3	The Observed Galaxy Overdensity	5
<b>3</b>	<b>Overview of Previous Analyses</b>	<b>6</b>
<b>4</b>	<b>Flux and Volume Limited Samples</b>	<b>7</b>
4.1	The Limits	7
4.2	Flux-limited Samples	7
4.3	Volume-limited Samples	8
<b>5</b>	<b>The Observed Angular Power Spectrum</b>	<b>9</b>
<b>6</b>	<b>Conclusion</b>	<b>15</b>
	<b>Acknowledgements</b>	<b>16</b>
<b>A</b>	<b>The Number-count and the Magnification Overdensities</b>	<b>16</b>
A.1	The metric	16
A.2	The density distortion	17
A.3	The volume distortion	18
A.4	The magnification distortion	19

---

## 1 Introduction

In recent years, relativistic effects [1–50] have been vastly studied. A number of the studies in the literature have shown how to calculate the observed clustering overdensity of galaxies in a relativistic context, i.e. the relativistic galaxy overdensity [1–11], revealing relativistic corrections to the simple “Newtonian” calculation that is standard for low redshift, small area surveys. Galaxy surveys with large volume coverage—spanning scales nearly and larger than the Hubble radius, reaching high redshifts—require relativistic corrections to the observed overdensity. Basically, these corrections are owing to the large-scale effects of (i) the gravitational potential, both local at the observed galaxies and also along the line of sight, and (ii) peculiar velocities, by the apparent motion of the galaxies relative to the observer. Together, these constitute the so-called “relativistic effects”.

Current optical surveys only cover low redshifts and sky area with dimensions which are smaller than the Hubble radius; thus, containing negligible relativistic effects. However, upcoming surveys in the optical and the radio/infrared, will extend to high redshifts and encompass large sky area—with dimensions equal and larger than the Hubble radius—providing deeper and richer information on the observable universe but, most importantly, on cosmological scales at the survey redshifts. On these scales, the relativistic effects become significant. These effects can, e.g. provide a means for a sensitive probe of the nature of dark energy

and modified gravity: by comparing the predictions from the relativistic corrections to the observation of the forthcoming surveys.

There are two fundamental issues underlying the relativistic analysis: Firstly, we need to correctly identify the galaxy overdensity that is observed on the past light cone; secondly, we need to account for all the distortions arising from observing on the past light cone, including redshift and volume perturbations (with all relativistic effects included) [6]. These relativistic effects appear in the power spectrum of matter in redshift space. However, all of these effects together can suitably be accounted for—simply by using the fact that the physical (observed) number of the galaxies depends on two main quantities: the survey *volume* and the apparent *flux* of the sources.

In this work we rely on the dependence of the physical galaxy number on the survey volume and the apparent flux, to re-trace the known relativistic galaxy overdensity (at first order perturbation). We recover all previously calculated terms and, still uncover subtle, yet crucial (background) parameters which are missed out by previous works. We start by re-calculating the relativistic galaxy overdensity—while revealing the new parameters—in Sec. 2; we relate our results to some previous works in Sec. 3. In Sec. 4 we give an overview of specific (flux- and volume-limited) samples of galaxy surveys and, in Sec. 5 we demonstrate the possible implications of the new parameters on the large-scale prediction of galaxy clustering, via the galaxy power spectrum, in the standard concordance model. We conclude in Sec. 6.

## 2 The Relativistic Galaxy Overdensity

In cosmological surveys, observers usually look at a certain volume  $v(\mathbf{n}, z)$  of the sky through a solid angle  $\Omega_{\mathbf{n}}$  in a given direction  $-\mathbf{n}$ , at a redshift  $z$  away. Apart from the redshift, the solid angle and the intrinsic properties of the observed sources, surveys will generically also depend on cosmic magnification via the apparent flux  $F(\mathbf{n}, z)$  (or luminosity) of the observed sources [5, 6, 12]. The observed flux of a source is inherently (de)amplified in an inhomogeneous universe. (Hereafter, we use “magnification” to mean *magnification of sources*, by the amplification of their flux and/or angular size.) Thus, the physical number  $N$  of galaxies observed in an *arbitrary* survey will depend on two main quantities which are, the observed sky volume  $v$  and the apparent flux  $F$  of the galaxies: i.e.  $N(\mathbf{n}, z) = N(v(\mathbf{n}, z), F(\mathbf{n}, z))$ .

Moreover, a generic sample of cosmic objects in the sky would intrinsically contain both “magnified” and “unmagnified” fractions, respectively; where the magnified fraction is proportional to the magnification bias. However, the actual measurable quantity—being the number of objects per unit solid angle per redshift—would consist of all the events together, with no distinctions between these fractions. Nevertheless, these fractions can each be isolated by observations and measured separately, given that the unmagnified fraction is volume-dependent and the magnified fraction is flux-dependent.

### 2.1 The Cumulative Number Densities

The ensemble average number of galaxies per unit volume per unit flux, is given by

$$\Theta = \frac{\partial^2 N(v, F)}{\partial v \partial F}, \quad (2.1)$$

which implicitly measures the *flux (or luminosity) function*. The ensemble average number of galaxies per unit volume—with flux in the infinitesimal range from  $F$  to  $F + dF$ —is given

by  $\Theta dF$ . Similarly,  $\Theta dv$  gives the ensemble average number per unit flux, of galaxies with distance (or position) within the volume element from  $v$  to  $v + dv$ .

Henceforth, it is taken that all quantities are given in redshift space, with a tilde being used only on quantities of interest to denote this. The *cumulative* number of sources per unit (observed) volume  $\tilde{n}_g$  is then computed by

$$\tilde{n}_g(v) = \int_{F_{\text{cut}}}^{F_*} dF \Theta(v, F), \quad (2.2)$$

where  $F_{\text{cut}} = F(m_{\text{cut}})$  is the instrument threshold or cut-off flux, with apparent magnitude  $m_{\text{cut}}$ . We note that  $\tilde{n}_g(v) = \tilde{n}_g(v|F=F_*)$  is the galaxy number counts in a unit volume, computed at a fixed flux  $F_*$ . In an inhomogeneous universe, the flux change  $dF$  will acquire perturbations; however, by integrating within fixed limits,  $F_{\text{cut}} < F \leq F_*$ , any resulting perturbation terms coming directly from  $dF$  must vanish (as surface terms). Thus,  $\tilde{n}_g$  inherits perturbations only arising in  $\Theta$ —indirectly by  $v$  and  $F$ .

Similarly, the *cumulative* number of sources per unit apparent flux  $\tilde{n}_F$  is given by

$$\tilde{n}_F(F) = \int_{v_{\text{min}}}^{v_*} dv \Theta(v, F), \quad (2.3)$$

where  $v_{\text{min}} = v(\tilde{r}_{\text{min}})$  is the initial volume at a given minimum distance  $\tilde{r}_{\text{min}}$  and,  $v_* = v(\tilde{r}_*)$  is the final volume at a given maximum distance  $\tilde{r}_*$ . Also,  $\tilde{n}_F(F) = \tilde{n}_F(v=v_*|F)$  is the galaxy number counts by a unit flux, computed at a fixed volume  $v_*$  and, by integrating within fixed limits,  $v_{\text{min}} \leq v \leq v_*$ , any resulting perturbations coming directly from  $dv$  will vanish—resulting in the perturbations in  $\tilde{n}_F$  arising only via  $\Theta$ .

Surveys like the SDSS<sup>1</sup> [51] and the LCRS<sup>2</sup> [52, 53], among others, employ two flux cut-offs: the instrument threshold (lower bound) below which source detection is cut off and, a certain maximum (upper bound) above which no source is detected. Thus, only sources with apparent magnitude in a given closed interval—in a specified sky volume—are measured. Usually, the given volume will also be demarcated by two distance (lower and upper) limits.

## 2.2 The Galaxy Number per Unit Solid Angle per Redshift

A volume element vector  $d\mathbf{v}$  and flux element vector  $d\mathbf{F}$  will result in a number of sources, which is given by the resultant number vector  $d\mathbf{N}$ , given by

$$d\mathbf{N} = \tilde{n}_g d\mathbf{v} + \tilde{n}_F d\mathbf{F}, \quad (2.4)$$

where  $\tilde{n}_g$  and  $\tilde{n}_F$  are scalar functions. We note that, given (2.1)–(2.3), the vector component  $\tilde{n}_g d\mathbf{v}$  is independent of flux and, the vector component  $\tilde{n}_F d\mathbf{F}$  is independent of volume. Thus, the magnitude  $dN$  of the resultant number (element) vector is given by

$$\begin{aligned} dN^2 &= d\mathbf{N} \cdot d\mathbf{N} = \tilde{n}_g^2 d\mathbf{v} \cdot d\mathbf{v} + \tilde{n}_F^2 d\mathbf{F} \cdot d\mathbf{F}, \\ &= \left\{ \left( \tilde{n}_g \tilde{\mathcal{V}} \right)^2 + \left( \tilde{n}_F \tilde{\mathcal{F}} \tilde{q}_\chi \right)^2 \right\} \left( d\Omega_{\mathbf{n}} dz \right)^2, \\ &\equiv \tilde{\mathcal{N}}_g^2 \left( d\Omega_{\mathbf{n}} dz \right)^2, \end{aligned} \quad (2.5)$$

<sup>1</sup><http://www.sdss.org/surveys/>

<sup>2</sup><http://qold.astro.utoronto.ca/~lin/lcrs.html>

where,

$$d\mathbf{v} = \mathbf{e}_v dv = \mathbf{e}_v \tilde{\mathcal{V}} d\Omega_{\mathbf{n}} dz, \quad (2.7)$$

with  $\mathbf{e}_v$  being the (orthonormal) volume unit vector,  $dv$  being the magnitude of  $d\mathbf{v}$  and,  $\tilde{\mathcal{V}} = \partial v / (\partial \Omega_{\mathbf{n}} \partial z)$  being the volume per unit solid angle per redshift. We assume a general scenario where the survey also pertains the apparent size  $\mathcal{X}$  of the sources, hence the observed flux depends on the apparent size of the sources, i.e.  $F(\mathbf{n}, z) = F(\mathcal{X}(\mathbf{n}, z))$ , and we have

$$d\mathbf{F} = -\mathbf{e}_F dF = -\mathbf{e}_F \tilde{\mathcal{F}} \tilde{q}_{\mathcal{X}} d\Omega_{\mathbf{n}} dz, \quad (2.8)$$

where  $\mathbf{e}_F$  is the (orthonormal) flux unit vector,  $dF$  is the magnitude of  $d\mathbf{F}$ ,  $\tilde{\mathcal{F}} = \partial F / \partial \mathcal{X}$  is the flux change per source size interval  $d\mathcal{X}$  (i.e. flux per unit size) and,  $\tilde{q}_{\mathcal{X}} = \partial \mathcal{X} / (\partial \Omega_{\mathbf{n}} \partial z)$  is the source size per unit solid angle per redshift. (Notice that the product  $\tilde{\mathcal{F}} \tilde{q}_{\mathcal{X}}$ , gives the flux per unit solid angle per redshift.) The quantity  $\tilde{n}_g dv$  (being the magnitude of the vector  $\tilde{n}_g d\mathbf{v}$ ) is actually the number of galaxies contained in the physical volume element  $dv$ —arising solely owing to the volume variation—and,  $\tilde{n}_F dF$  (being the magnitude of the vector  $\tilde{n}_F d\mathbf{F}$ ) is the number of galaxies arising solely owing to the change  $dF$  in apparent flux.

Thus, given (2.4)–(2.8), we have the (physical) number of galaxies per unit solid angle per redshift—which is actually what observers measure—given by

$$\begin{aligned} \tilde{\mathcal{N}}_g(\mathbf{n}, z) &= \left\{ \left[ \tilde{n}_g(\mathbf{n}, z) \tilde{\mathcal{V}}(\mathbf{n}, z) \right]^2 + \left[ \tilde{n}_F(\mathbf{n}, z) \tilde{\mathcal{F}}(\mathbf{n}, z) \tilde{q}_{\mathcal{X}}(\mathbf{n}, z) \right]^2 \right\}^{\frac{1}{2}}, \\ &= \langle \tilde{\mathcal{N}}_g \rangle(\bar{z}) \left\{ 1 + \epsilon_v^2(\bar{z}) \left[ \frac{\delta \tilde{n}_g(\mathbf{n}, z)}{\bar{n}_g(\bar{z})} + \frac{\delta \tilde{\mathcal{V}}(\mathbf{n}, z)}{\bar{\mathcal{V}}(\bar{z})} \right] + \epsilon_{\mathcal{F}}^2(\bar{z}) \mathcal{Q}(\bar{z}) \frac{\delta \tilde{\mathcal{F}}(\mathbf{n}, z)}{\bar{\mathcal{F}}(\bar{z})} \right\}, \end{aligned} \quad (2.9)$$

where for the second equality (and henceforth) first-order perturbations are assumed, i.e.  $\delta \tilde{X} = \tilde{X} - \bar{X}$  is the perturbation in a given quantity  $\tilde{X}$ , with  $|\delta \tilde{X}| \ll 1$  and overbars denote “background” quantities, averaged over all solid angles. The redshift distribution of the galaxies is obtained by averaging over all solid angles, given by  $d\bar{N}(\bar{z}) = \langle \tilde{\mathcal{N}}_g \rangle(\bar{z}) dz$ , where

$$\begin{aligned} \langle \tilde{\mathcal{N}}_g \rangle^2 &= (\bar{n}_g \bar{\mathcal{V}})^2 + (\bar{n}_F \bar{\mathcal{F}} \bar{q}_{\mathcal{X}})^2, \\ &= (\epsilon_v^2 + \epsilon_{\mathcal{F}}^2) \langle \tilde{\mathcal{N}}_g \rangle^2, \end{aligned} \quad (2.10)$$

is the square of the average galaxy distribution density in redshift space. The parameters  $\epsilon_v \equiv \bar{n}_g \bar{\mathcal{V}} / \langle \tilde{\mathcal{N}}_g \rangle$  and  $\epsilon_{\mathcal{F}} \equiv \bar{n}_F \bar{\mathcal{F}} \bar{q}_{\mathcal{X}} / \langle \tilde{\mathcal{N}}_g \rangle$  are the fractional contributions by the change in volume and the change in flux, respectively, in the background sample. That is, if the survey volume and the apparent flux are variable, then the change in volume will contribute a certain fraction  $\epsilon_v$  in the average distribution density  $\langle \tilde{\mathcal{N}}_g \rangle$  and, similarly, the variation in flux will also contribute a fraction  $\epsilon_{\mathcal{F}}$ . By (2.10), the two fractions give the identity

$$\epsilon_v^2(\bar{z}) + \epsilon_{\mathcal{F}}^2(\bar{z}) = 1, \quad (2.11)$$

where for fixed-volume surveys (at fixed  $z$ )  $\bar{\mathcal{V}} = 0$ , which implies  $\epsilon_v = 0$  and the entire background sample is generated by the variation in flux, with  $\epsilon_{\mathcal{F}} = \bar{n}_F \bar{\mathcal{F}} \bar{q}_{\mathcal{X}} / \langle \tilde{\mathcal{N}}_g \rangle = 1$ . Consequently, this sample is ideal for (pure) magnification analysis, see e.g. [12]. Fixing the apparent flux—and/or size—leads to  $\bar{\mathcal{F}} \bar{q}_{\mathcal{X}} = 0$  and hence  $\epsilon_{\mathcal{F}} = 0$ , with  $\epsilon_v = \bar{n}_g \bar{\mathcal{V}} / \langle \tilde{\mathcal{N}}_g \rangle = 1$ ; thus, corresponding to a (pure) number-count analysis, see e.g. [3, 8, 11].

The parameter  $\mathcal{Q}$  is the cosmic *magnification bias* [5, 6, 12, 54–59], given by

$$\mathcal{Q} \equiv \left. \frac{\partial \ln \tilde{\mathcal{N}}_F}{\partial \ln \tilde{\mathcal{F}}} \right|_{\bar{z}} = \frac{1}{2} (2 + 2s_{\mathcal{X}} - 5s_F), \quad (2.12)$$

where we have denoted  $\tilde{\mathcal{N}}_F = \bar{n}_F \tilde{\mathcal{F}} \bar{q}_{\mathcal{X}}$ , and  $s_{\mathcal{X}} \equiv \partial \ln \bar{q}_{\mathcal{X}} / \partial \ln \tilde{\mathcal{F}}$  is the *size bias* [55–57]; with the parameter  $s_F \equiv -(2/5) \partial \ln \bar{n}_F / \partial \ln \tilde{\mathcal{F}} = \partial \log_{10} \bar{n}_F / \partial \bar{m}$  corresponding to a *flux bias* [53] and,  $m$  is the apparent magnitude. For a given source, the surface brightness  $\mathcal{S} \propto (F/\mathcal{X}^2)$  is a constant and, is unaffected by cosmic amplification (or magnification) of the source [55]. This implies that  $\bar{F}/\bar{\mathcal{X}}^2 = \text{constant}$ , and we get  $2s_{\mathcal{X}} = \partial \ln \bar{q}_{\mathcal{X}} / \partial \ln \bar{\mathcal{X}}$ . However, note that if the survey does not pertain the apparent size of the source, we will have in (2.9) that  $\tilde{n}_F \tilde{\mathcal{F}} \tilde{q}_{\mathcal{X}} \rightarrow \tilde{n}_F \tilde{\mathcal{F}}$  and thus  $\tilde{\mathcal{N}}_F = \tilde{n}_F \tilde{\mathcal{F}}$ , where  $\tilde{\mathcal{F}}$  now becomes the change in flux per unit solid-angle change per redshift change. Consequently,  $s_{\mathcal{X}} = 0$  and we have  $2\mathcal{Q} = 2 - 5s_F$ . Thus (2.12) generalizes the cosmic magnification bias—in the light of previous works.

### 2.3 The Observed Galaxy Overdensity

The total observed, relativistic galaxy overdensity, given (2.9), is given by

$$\Delta_{\mathbf{g}}^{\text{obs}}(\mathbf{n}, z) \equiv \frac{\tilde{\mathcal{N}}_{\mathbf{g}}(\mathbf{n}, z) - \langle \tilde{\mathcal{N}}_{\mathbf{g}} \rangle(\bar{z})}{\langle \tilde{\mathcal{N}}_{\mathbf{g}} \rangle(\bar{z})}, \quad (2.13)$$

$$= \epsilon_{\mathbf{v}}^2(\bar{z}) \left( \tilde{\delta}_{\mathbf{g}}(\mathbf{n}, z) + \tilde{\delta}_{\mathbf{v}}(\mathbf{n}, z) \right) + \epsilon_{\mathcal{F}}^2(\bar{z}) \mathcal{Q}(\bar{z}) \tilde{\delta}_{\mathcal{M}}(\mathbf{n}, z), \quad (2.14)$$

where  $\tilde{\delta}_{\mathbf{g}} \equiv \delta \tilde{n}_{\mathbf{g}} / \bar{n}_{\mathbf{g}}$  is the number density contrast and,  $\tilde{\delta}_{\mathbf{v}} \equiv \delta \tilde{\mathcal{V}} / \bar{\mathcal{V}}$  is the volume density contrast. In the last line in (2.14) we have used that for magnified sources, the flux per unit source size—in the background—is proportional to the underlying magnification per unit source size, i.e.  $\tilde{\mathcal{F}} \propto \tilde{\mathcal{M}}$ , and we have  $\partial \ln \tilde{\mathcal{F}} = \partial \ln \tilde{\mathcal{M}}$ . Consequently, we get the magnification contrast  $\tilde{\delta}_{\mathcal{M}} \equiv \delta \tilde{\mathcal{M}} / \tilde{\mathcal{M}} = \delta \tilde{\mathcal{F}} / \tilde{\mathcal{F}}$ . (Note that, given  $\tilde{\mathcal{F}} \propto \tilde{\mathcal{M}}$  we get  $\tilde{\mathcal{F}} = \tilde{\mathcal{M}}/\nu$  at first order perturbations, where the factor  $\nu = \tilde{\mathcal{M}}/\bar{\mathcal{M}}$  quantifies the cosmic (de)magnification—see e.g. [12].)

The relativistic *number-count overdensity* (see Appendix A for details) is given by,

$$\begin{aligned} \Delta_n^{\text{obs}}(\mathbf{n}, z) &\equiv \tilde{\delta}_{\mathbf{g}}(\mathbf{n}, z) + \tilde{\delta}_{\mathbf{v}}(\mathbf{n}, z), \quad (2.15) \\ &= \Delta_{\mathbf{g}}(\mathbf{n}, z) - \frac{1}{\mathcal{H}(\bar{z})} \partial_r V_{\parallel}(\mathbf{n}, z) + \int_0^{\bar{r}_S} d\bar{r} \left[ \frac{2}{\bar{r}_S} - (\bar{r}_S - \bar{r}) \frac{\bar{r}}{\bar{r}_S} \nabla_{\perp}^2 \right] (\Phi + \Psi)(\mathbf{n}, \bar{r}) \\ &+ \left( b_e(\bar{z}) - \frac{\mathcal{H}'(\bar{z})}{\mathcal{H}^2(\bar{z})} - \frac{2}{\bar{r}_S \mathcal{H}(\bar{z})} \right) \left[ V_{\parallel}(\mathbf{n}, z) + \int_0^{\bar{r}_S} d\bar{r} (\Phi' + \Psi')(\mathbf{n}, \bar{r}) \right] \\ &+ \frac{1}{\mathcal{H}(\bar{z})} \Psi'(\mathbf{n}, z) - \left( b_e(\bar{z}) - 1 - \frac{\mathcal{H}'(\bar{z})}{\mathcal{H}^2(\bar{z})} - \frac{2}{\bar{r}_S \mathcal{H}(\bar{z})} \right) \Phi(\mathbf{n}, z) \\ &+ [3 - b_e(\bar{z})] \mathcal{H}(\bar{z}) V(\mathbf{n}, z) - 2\Psi(\mathbf{n}, z), \quad (2.16) \end{aligned}$$

where  $V_{\parallel} = -\mathbf{n} \cdot \mathbf{V} = \partial_r V$  is the line-of-sight component of the peculiar velocity, with  $V$  being a gauge-invariant velocity potential;  $\bar{r}_S = \bar{r}(z_S)$  is the radial comoving distance at the redshift  $z_S$  of the source from the observer,  $\mathcal{H}$  is the comoving Hubble parameter,  $b_e$  is the galaxy evolution bias,  $\Phi$  and  $\Psi$  are the gauge-invariant temporal and spatial gravitational metric potentials, respectively and,  $\nabla_{\perp}^2$  is the transverse, image-plane Laplacian. In this section, and Appendix A, a prime denotes derivative with respect to conformal time  $\eta$ .

The relativistic *magnification overdensity* (see Appendix A for details) is given by

$$\Delta_{\mathcal{M}}^{\text{obs}}(\mathbf{n}, z) \equiv \mathcal{Q}(\bar{z})\tilde{\delta}_{\mathcal{M}}(\mathbf{n}, z), \quad (2.17)$$

$$\begin{aligned} &= 2\mathcal{Q}(\bar{z})\left(1 - \frac{1}{\bar{r}_s\mathcal{H}(\bar{z})}\right)\left[\Phi(\mathbf{n}, z) - V_{\parallel}(\mathbf{n}, z) - \int_0^{\bar{r}_s} d\bar{r}(\Phi' + \Psi')(\mathbf{n}, \bar{r})\right] \\ &+ 2\mathcal{Q}(\bar{z})\Psi(\mathbf{n}, z) - \mathcal{Q}(\bar{z})\int_0^{\bar{r}_s} d\bar{r}\left[\frac{2}{\bar{r}_s} - (\bar{r}_s - \bar{r})\frac{\bar{r}}{\bar{r}_s}\nabla_{\perp}^2\right](\Phi + \Psi)(\mathbf{n}, \bar{r}), \end{aligned} \quad (2.18)$$

where notations are as in (2.16). Notice that the overdensities  $\Delta_n^{\text{obs}}$  and  $\Delta_{\mathcal{M}}^{\text{obs}}$ —which are, separately, observable—are volume  $v$  and flux  $F$  dependent, respectively. (The methods given by e.g. [12, 55, 60, 61] can be applied to measure  $\Delta_{\mathcal{M}}^{\text{obs}}$ .) Thus,  $\Delta_{\mathcal{M}}^{\text{obs}}$  and  $\Delta_n^{\text{obs}}$  essentially comprise the “magnified” and the “unmagnified” parts, respectively, of the relativistic overdensity (2.13). We then simplify the total observed, relativistic overdensity (2.14), given by

$$\Delta_g^{\text{obs}}(\mathbf{n}, z) = \epsilon_{\mathcal{V}}^2(z)\Delta_n^{\text{obs}}(\mathbf{n}, z) + \epsilon_{\mathcal{F}}^2(z)\Delta_{\mathcal{M}}^{\text{obs}}(\mathbf{n}, z). \quad (2.19)$$

where  $\Delta_n^{\text{obs}}(\mathbf{n}, z)$  and  $\Delta_{\mathcal{M}}^{\text{obs}}(\mathbf{n}, z)$  are given by (2.16) and (2.18), respectively.

The parameters  $\epsilon_{\mathcal{V}}$  and  $\epsilon_{\mathcal{F}}$  have never previously been taken into account—in the literature—in the calculation of the observed, relativistic galaxy overdensity (2.19). Thus, the calculations in (2.4)–(2.19) provide the correct, fully self-consistent approach for combining the unmagnified (volume-dependent) and the magnified (flux-dependent) relativistic components of the observed overdensity of galaxy surveys. Note that the observed, relativistic overdensity (2.19) is unique and physically defined: it does not correspond to any of the standard gauge-invariant definitions of overdensity, but it is automatically gauge-invariant [13].

### 3 Overview of Previous Analyses

It should be pointed out that previous works [3–11] have, by implication, applied the splitting of a galaxy sample into two separate “volume-dependent” and “flux-dependent” parts. The only difference is that (keeping in mind the difference in notation) in the previous works, the two respective parts are first computed *individually* and later merely summed directly. However, doing so is inconsistent.

For example, in the work by [5]—sections *C*, *D* and *E* (see also [4, 6–10])—the relativistic overdensity  $\Delta_g^{\text{obs}}$  is computed in two parts: Firstly, the pure number-count overdensity “ $\tilde{\delta}_g(\text{no mag})$ ” is computed (see particularly, (40)–(55), by [5]), accounting for the overdensity solely owing to the change in the observed volume. Afterwards, by using that most real cosmic samples also depend on the apparent flux from the sources, the contribution solely owing to the variation in flux “ $\mathcal{Q}\delta\mathcal{M}$ ” is then added (see (60), by [5]), given by

$$\tilde{\delta}_g = \tilde{\delta}_g(\text{no mag}) + \mathcal{Q}\delta\mathcal{M}, \quad (3.1)$$

where the various terms in this equation are given in the same notation as [5]. We readily identify  $\tilde{\delta}_g(\text{no mag}) := \Delta_n^{\text{obs}}$  and  $\mathcal{Q}\delta\mathcal{M} := \Delta_{\mathcal{M}}^{\text{obs}}$ . Consequently, (3.1) directly implies  $\epsilon_{\mathcal{V}}^2 = 1 = \epsilon_{\mathcal{F}}^2$ , which is misleading. In [3], only  $\Delta_n^{\text{obs}}$  (2.15) is calculated, and without taking the evolution bias  $b_e$  into account. Whereas in [4] (noting difference in notation),  $\Delta_n^{\text{obs}}$  and  $\Delta_{\mathcal{M}}^{\text{obs}}$  were individually computed, separately, and then summed directly—like in [5]. (It should be noted that the results by [3] and by [4], respectively, are both recovered by the work of [5].)

However, given that the physical number of sources  $N$  implicitly depends on both the survey volume and the sources’ apparent flux, then we have the sources’ number element  $dN$  to be fully decomposed by (2.4) into the respective independent components; thus leading to (2.11) and (2.19). This way, i.e. by the approach via (2.4), we are able to obtain a consistent procedure for including the true effect,  $\mathcal{Q}\tilde{\delta}_{\mathcal{M}}$ , of cosmic magnification in the relativistic overdensity. Equation (2.19) and hence, the entire analysis in Sec. 2, generalize the relativistic overdensity for a *generic* survey, in which both the survey volume and the instrument flux are variable (within given intervals). Specifically, in redshift surveys (see [51–53]), as well as continuum surveys (see [22]), the instrument is fixed at a particular flux or intensity limit and, only above such limit can sources be detected. Such surveys are called, “threshold surveys,” with the given limit being the instrument’s “threshold.”

Essentially, (2.19) implies that—contrary to previous analyses (see [4–10])—the volume-dependent and the flux-dependent parts, respectively, of the generic relativistic overdensity do not merely add; they are scaled down by squares of their respective fractional contribution in the (total) redshift-space average distribution density.

## 4 Flux and Volume Limited Samples

An generic survey would involve variable volume and flux, respectively. Thus, as previously mentioned, the generated catalogue of the cosmic objects would inherently contain both “magnified” (flux-dependent) and “unmagnified” (volume-dependent) fractions, respectively; with the observationally measurable quantity, being the number of objects per unit solid angle per redshift, consisting of all the events together without any distinctions between these fractions. However, in practice, analyses may be done for specific samples; usually, for either flux-limited or volume-limited samples. (These sample types are discussed subsequently.) In order to construct or extract these samples, certain measurement limits are defined.

### 4.1 The Limits

The principal limiting parameters are usually the apparent flux and the observed (geometric) cosmic depth. These parameters invariably determine the source intrinsic brightness, i.e. luminosity. The flux is prescribed by an apparent magnitude  $m$  and, the luminosity is given by an absolute magnitude  $M$ .

Basically, once the apparent magnitude limit  $m_{\text{lim}}$  is specified, the limit on the absolute magnitude is readily determined (via the magnitude–distance relation), given by

$$M_{\text{lim}} = m_{\text{lim}} - 25 - 5 \log_{10}(D_{\text{lim}}), \quad (4.1)$$

where  $D_{\text{lim}} = \tilde{r}(z_{\text{lim}}) \leq \tilde{r}_*$  is the cosmic depth, being the (background) physical distance along the line of sight measured in Mpc, at a given maximum redshift  $z_{\text{lim}}$ ; with  $m_{\text{lim}} = m_{\text{cut}}$ . Note that in reality,  $M_{\text{lim}}$  may be affected by the well-known  $K$ -correction, galactic extinction, and other notable effects—especially if  $D_{\text{lim}}$  is large, i.e. at a high  $z$ —thus, a more general expression for  $M_{\text{lim}}$  will need to incorporate these effects [62].

### 4.2 Flux-limited Samples

In flux-limited samples, the measuring instrument is operated on a fixed flux value—serving as the instrument’s threshold—and, only sources with flux strictly above this threshold are

detected or extracted. The flux limit is fixed by the apparent magnitude limit  $m_{\text{lim}}$  and, sources intrinsically brighter (i.e.  $M < M_{\text{lim}} < 0$ ) than the absolute limit (4.1), are extracted:

$$M = m_{\text{lim}} - 25 - 5 \log_{10}(\tilde{r}), \quad (4.2)$$

where we notice that the absolute magnitude  $M$  is mainly a function of the background (line-of-sight) physical distance  $\tilde{r}$ —and, the sources are accessed by varying the distance. However, the distance is in turn a function  $\tilde{r} = \tilde{r}(z)$  of redshift  $z$ , so that computing  $\tilde{r}$  first requires knowing the actual redshift. Therefore, the experiment needs to have the sufficient resolution and sensitivity to determine  $z$ . This way, the individual sources are differentiated, and their actual number is counted. In flux-limited surveys, the instrument is able to pick out the individual sources. Thus the given survey is automatically a “number-count” survey. (Invariably, the survey is also a “redshift” survey, with the catalogue consisting of sky positions and luminosities of the sources.)

Note that, by having a flux threshold, it implies that sources at higher redshifts must have higher luminosities in order to be detected by the instrument, i.e. sources at larger  $\tilde{r}$  must have lower  $M$ . (Otherwise, they lead to a flux which is lower than the given instrument threshold, and are therefore filtered out.) In fact, once the magnitude limit is applied, the flux becomes irrelevant; the instrument no longer measures the variation in flux—it only registers the number of the individual sources which have flux above the (instrument) threshold. Thus, the background *change in flux per unit solid angle per redshift*, is zero (i.e.  $\bar{\mathcal{F}}\bar{q}_x = 0$ ); hence  $\epsilon_{\mathcal{F}} = 0$  and, given (2.11), we have  $\epsilon_{\mathcal{V}} = 1$ . Then by (2.19), the given distribution is adequately described by  $\Delta_n^{\text{obs}}$ . (Appropriate for pure number-count analysis only, see e.g. [3, 8, 11].)

Moreover, it should be noted that in order to extract or screen for the required sources, the instrument is fixed at the limit  $m_{\text{lim}}$ ; however, in order to determine the number (density) of these sources, the integral in (2.2) must be evaluated within  $m_* \leq m < m_{\text{lim}}$  (noting that a higher flux corresponds to a lower apparent magnitude). Consequently, the resulting distribution density depends on the sources’ distance, and hence, on the sky volume  $v(\tilde{r})$  containing  $\tilde{r}$ , at redshift  $z$ . Given (4.2), physically it implies that intrinsically faint sources will not be detected by the the instrument, unless they are close enough; whereas, brighter sources are detected even at large distances away. This creates a gradient in the number density with distance. Thus, the given sample is *spatially not uniform* [62].

### 4.3 Volume-limited Samples

An ideal volume-limited survey would be one done by observing a *fixed patch* of the sky at a specified redshift, and the flux and/or size distribution on the given sky patch is mapped. Thus, at the given redshift, the background *change in volume per unit solid angle per redshift*, is zero (i.e.  $\bar{\mathcal{V}} = 0$ ); consequently,  $\epsilon_{\mathcal{V}} = 0$  and  $\epsilon_{\mathcal{F}} = 1$ . Similarly, given (2.19), the generated sample is adequately described by  $\Delta_{\mathcal{M}}^{\text{obs}}$ . (Such a survey would be appropriate for pure magnification analysis—see e.g. [12, 61].)

However, volume-limited samples may also be extracted from flux-limited samples. This is usually done by specifying a maximum depth  $D_{\text{lim}}$  (at a fixed redshift  $z_{\text{lim}} \leq z_*$ ), prescribing the volume  $v_{\text{lim}} = v(D_{\text{lim}})$  of interest and, similarly, picking out only sources that are intrinsically brighter than  $M_{\text{lim}} < 0$ —with luminosities specified by an absolute magnitude:

$$M = m - 25 - 5 \log_{10}(D_{\text{lim}}), \quad (4.3)$$

where we note that the absolute magnitude  $M = M(m)$  is mainly a function of the apparent magnitude  $m$ , and hence, the flux (density). Here, the sources are accessed by varying the

apparent magnitude. Obviously, the cosmic depth  $D_{\text{lim}}$  is essentially the limiting radius of the sample volume—with the given sources being at particular distances  $\check{r}_{\text{min}} \leq \check{r} \leq D_{\text{lim}}$ .

We notice that, given (4.3), in volume-limited samples the flux limit is no longer present and, all *possible* fluxes are mapped (within the specified cosmic volume). The extracted sample is *spatially uniform*, in the sense that the gradient of the number density vanishes, since the number density of the given sample does not vary with distance [62].

## 5 The Observed Angular Power Spectrum

We investigate the angular power spectrum associated with (2.19), with the main goal of showing how the parameters  $\epsilon_{\mathcal{V}}$  and  $\epsilon_{\mathcal{F}}$  affect the predictions of the large scale structure. We avoided using any approximations, e.g. the Limber’s approximation [63] (for integral terms).

To probe the galaxy power spectrum, we assume the standard late-time  $\Lambda$ CDM universe: dominated by a cosmological constant  $\Lambda$  and cold dark matter (CDM); considering mainly the very large (linear) scales. We adopt the zero anisotropic stress metric given by

$$ds^2 = a^2 [-(1 + 2\Phi)d\eta^2 + (1 - 2\Phi)d\mathbf{x}^2], \quad (5.1)$$

i.e. with  $\Psi = \Phi$ . We relate the background galaxy (density) bias  $b$  to the background galaxy evolution bias  $b_e$ , given (see Appendix A) by [6]

$$b = 1 - \frac{1}{3}b_e. \quad (5.2)$$

Jeong et al [5] used a different approach to derive a relation between the two parameters. In the given reference, the authors assumed that the abundance of galaxies follows a universal mass function, and they work to obtain  $b = 1 + b_e/(\delta_c f)$ ; with  $\delta_c$  being the matter collapse density contrast and,  $f$  being the usual logarithmic matter growth rate. Note that in (5.2), we do not use any assumptions in the derivation—only the natural definition of the parameters.

We use the present-epoch matter density parameter  $\Omega_{m0} = 0.3$ , and the Hubble constant  $H_0 = 67.8 \text{ km}\cdot\text{s}^{-1}\cdot\text{Mpc}^{-1}$ , for all numerical computations. Furthermore, we adopt a vanishing evolution bias  $b_e = 0$ —a scenario where the galaxy do not evolve with time—which given (5.2), implies that the galaxy bias  $b = 1$ . For simplicity,  $\epsilon_{\mathcal{V}}$  and  $\epsilon_{\mathcal{F}}$  are assumed to be absolute constants. (A proper modelling of these parameters as functions of redshift  $z$ , may be crucial for proper observational analysis.)

On very large (linear) scales, the matter and the galaxy rest frames coincide (given the homogeneity and isotropy of these scales), and we can set the matter and the galaxy velocities—along the line of sight—to be equal:  $V_m^{\parallel} = V_{\parallel} = V_g^{\parallel}$ , i.e. galaxies follow trajectories that are parallel to that of the underlying matter (equivalently, the galaxies are comoving with the underlying matter); hence there is essentially no momentum (ex)change between the two frames to cause any bias between the velocities [6]. However, on small (non-linear) scales, the implicit assumption of the matter-galaxy velocity equality may fail; hence implying velocity biasing, which may need to be taken into account.

Given (2.19), the observed angular galaxy power spectrum (dropping all over-bars) is

$$\begin{aligned} C_{\ell}^{\text{obs}}(z_s) &= \epsilon_{\mathcal{V}}^4(z_s) C_{\ell}^{(n)}(z_s) + [1 - \epsilon_{\mathcal{V}}^2(z_s)]^2 C_{\ell}^{(\mathcal{M})}(z_s) \\ &+ 2\epsilon_{\mathcal{V}}^2(z_s) [1 - \epsilon_{\mathcal{V}}^2(z_s)] C_{\ell}^{(n,\mathcal{M})}(z_s), \end{aligned} \quad (5.3)$$

where we used (2.11), with  $C_\ell^{(n)}$  and  $C_\ell^{(\mathcal{M})}$  being the number-count and the magnification angular power spectra, respectively. Given the multipole expansion coefficients  $a_{\ell m}$ , we have

$$\begin{aligned} C_\ell^{(n)}(z_s) &= \left\langle |a_{\ell m}(z_s)|^2 \right\rangle, \\ &= \frac{4}{\pi^2} \left( \frac{9}{10} \right)^2 \int dk k^2 T(k)^2 P_{\Phi_p}(k) \left| f_\ell^{(n)}(k, z_s) \right|^2, \end{aligned} \quad (5.4)$$

where  $T(k)$  is the linear transfer function and  $P_{\Phi_p}(k)$  is the primordial power spectrum [64]; with  $|f_\ell^{(n)}|$  denoting the complex modulus of  $f_\ell^{(n)}$ , and

$$\begin{aligned} f_\ell^{(n)}(k, z_s) &= b(z_s) \tilde{\Delta}_m(k, z_s) j_\ell(kr_s) - j_\ell''(kr_s) \frac{1}{\mathcal{H}} \partial_r \tilde{V}_m^\parallel(k, z_s) + j_\ell(kr_s) \frac{1}{\mathcal{H}} \dot{\tilde{\Phi}}(k, z_s) \\ &+ (3 - b_e) \mathcal{H} \tilde{V}_m(k, z_s) j_\ell(kr_s) - \left( b_e - 1 - \frac{\mathcal{H}'}{\mathcal{H}^2} - \frac{2}{r_s \mathcal{H}} \right) \tilde{\Phi}(k, z_s) j_\ell(kr_s) \\ &+ \left( b_e - \frac{\mathcal{H}'}{\mathcal{H}^2} - \frac{2}{r_s \mathcal{H}} \right) \left[ j_\ell'(kr_s) \tilde{V}_m^\parallel(k, z_s) + 2 \int_0^{r_s} dr j_\ell(kr) \dot{\tilde{\Phi}}(k, r) \right] \\ &- 2 \tilde{\Phi}(k, z_s) j_\ell(kr_s) + \frac{2}{r_s} \int_0^{r_s} dr j_\ell(kr) \left[ 2 - \frac{(r - r_s)}{r} \ell(1 + \ell) \right] \tilde{\Phi}(k, r), \end{aligned} \quad (5.5)$$

where  $j_\ell$  is the spherical Bessel function and  $j_\ell'(kr) = \partial j_\ell(kr) / \partial(kr)$ ; in this section, particularly in (5.5) and (5.8), we use a dot to denote derivative with respect to  $\eta$ , for shortage of better notations. (Note that in Sec 2 and Appendix A, a prime is used to denote derivative with respect to  $\eta$ .) A tilde denotes  $\tilde{X}(k, z) \equiv X(k, z) / \Phi_d(k)$ , for a parameter  $X$ ;  $\Phi_d$  is the gravitational potential at the epoch of photon-matter decoupling  $z = z_d$ , and [6, 13, 38, 64]

$$\Phi(k, z_d) = \frac{9}{10} \Phi_p(k) T(k) \equiv \Phi_d(k), \quad (5.6)$$

where  $\Phi_p$  is the primordial gravitational potential. (See [64] for a numerical formula for  $T(k)$ .)

Similarly, the magnification angular power spectrum is given by

$$C_\ell^{(\mathcal{M})}(z_s) = \frac{4}{\pi^2} \left( \frac{9}{10} \right)^2 \int dk k^2 T(k)^2 P_{\Phi_p}(k) \left| f_\ell^{(\mathcal{M})}(k, z_s) \right|^2, \quad (5.7)$$

where notations are as in (5.4), and

$$\begin{aligned} f_\ell^{(\mathcal{M})}(k, z_s) &= -\frac{2\mathcal{Q}(z_s)}{r_s} \int_0^{r_s} dr j_\ell(kr) \left[ 2 - \frac{(r - r_s)}{r} \ell(\ell + 1) \right] \tilde{\Phi}(k, r) \\ &+ 2\mathcal{Q}(z_s) j_\ell(kr_s) \tilde{\Phi}(k, z_s) - \frac{4\mathcal{Q}(z_s)}{r_s} \int_0^{r_s} dr j_\ell(kr) \tilde{\Phi}(k, r) \\ &+ 2\mathcal{Q}(z_s) \left( 1 - \frac{1}{r_s \mathcal{H}(z_s)} \right) \left[ j_\ell(kr_s) \tilde{\Phi}(k, z_s) - j_\ell'(kr_s) \tilde{V}_m^\parallel(k, z_s) \right. \\ &\quad \left. - 2 \int_0^{r_s} dr j_\ell(kr) \dot{\tilde{\Phi}}(k, r) \right], \end{aligned} \quad (5.8)$$

where notations are as in (5.5); the cross angular power spectrum between  $\Delta_n^{\text{obs}}$  and  $\Delta_{\mathcal{M}}^{\text{obs}}$ , is

$$C_\ell^{(n\mathcal{M})}(z_s) = \frac{4}{\pi^2} \left( \frac{9}{10} \right)^2 \int dk k^2 T(k)^2 P_{\Phi_p}(k) \left| f_\ell^{(n\mathcal{M})}(k, z_s) \right|^2, \quad (5.9)$$

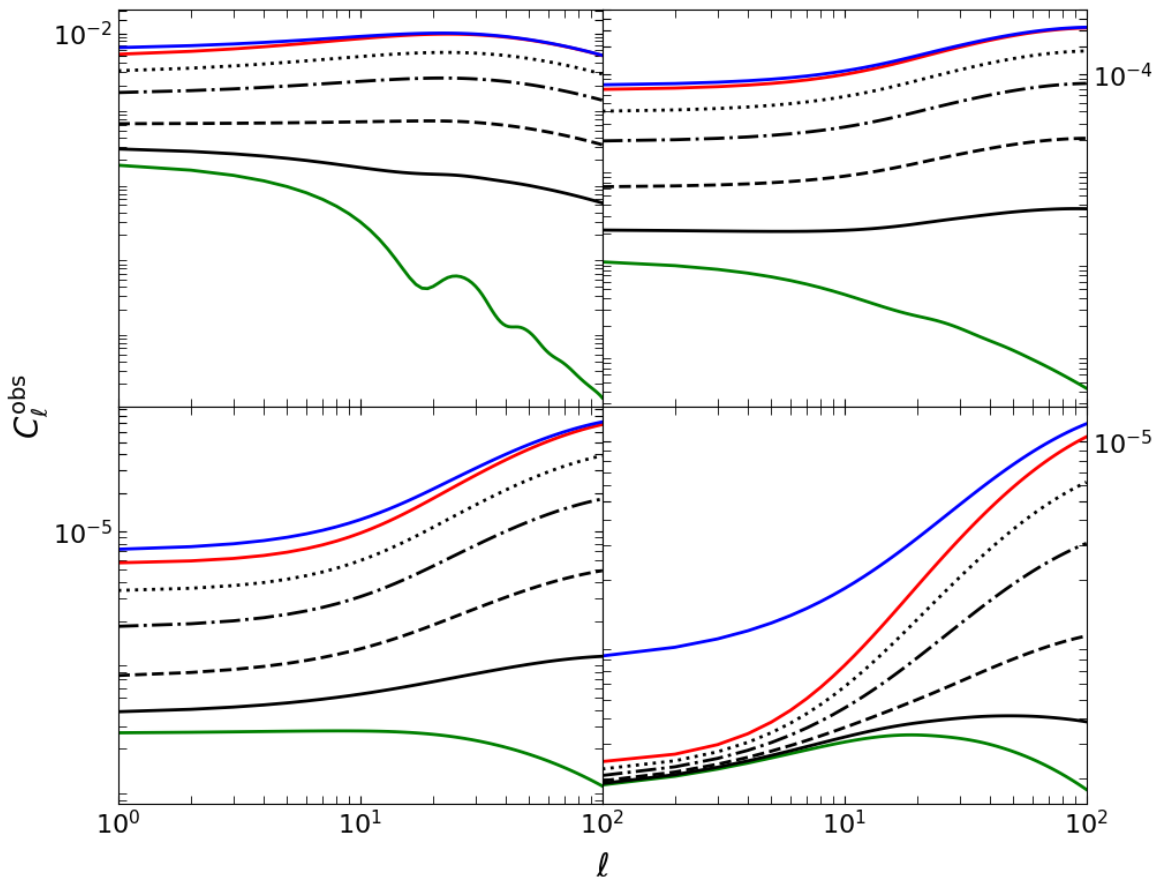


**Figure 1.** The plots of the angular power spectra for magnification bias  $\mathcal{Q} = 1$ , at the source redshifts:  $z_s = 0.1$  (top left),  $z_s = 0.5$  (top right),  $z_s = 1$  (bottom left) and  $z_s = 3$  (bottom right). The various lines show: the magnification angular power spectrum  $C_\ell^{(\mathcal{M})}$  (green); the full relativistic angular power spectrum  $C_\ell^{\text{obs}}$  with  $\epsilon_v^2 = 0.1$  and  $\epsilon_f^2 = 0.9$  (solid black),  $\epsilon_v^2 = 0.25$  and  $\epsilon_f^2 = 0.75$  (dashed black),  $\epsilon_v^2 = 0.5 = \epsilon_f^2$  (dot-dashed black) and,  $\epsilon_v^2 = 0.75$  and  $\epsilon_f^2 = 0.25$  (dotted black); the number-count power spectrum  $C_\ell^{(n)}$  (red). The blue line shows the result corresponding to previous works ( $\epsilon_v^2 = 1 = \epsilon_f^2$ ).

where we have  $f_\ell^{(n\mathcal{M})} = f_\ell^{(n)} \star f_\ell^{(\mathcal{M})*}$ , with  $\star$  denoting complex multiplication, the asterisk denoting complex conjugate and, other notations are as in (5.4).

In Fig. 1 we show plots of the total observed angular power spectrum  $C_\ell^{\text{obs}}$ , the observed number-count angular power spectrum  $C_\ell^{(n)}$  and the observed magnification angular power spectrum  $C_\ell^{(\mathcal{M})}$ : for magnification bias  $\mathcal{Q} = 1$ , at source redshifts  $z_s = 0.1, 0.5, 1$  and  $3$ . In this work we show the angular power spectra without the usual scaling factor,  $\ell(\ell+1)/(2\pi)$ , as widely used in the literature. Removing this factor allows the scale-dependent behaviour of the angular power spectra to display better. For illustrative purpose, in  $C_\ell^{\text{obs}}$  we adopted values for  $\epsilon_v$  and  $\epsilon_f$  such that (2.11) holds; however, we also considered the violated scenario where both parameters are unity, which corresponds to the results of previous works in the literature. We see that, for all the cases where (2.11) holds true, the total observed angular power spectrum is bounded by  $C_\ell^{(\mathcal{M})} \leq C_\ell^{\text{obs}} \leq C_\ell^{(n)}$  on all scales, at all the redshifts (for the given value of  $\mathcal{Q}$ ). Obviously, we see that  $\epsilon_v$  and  $\epsilon_f$  regulate the amplitude of  $C_\ell^{\text{obs}}$  on all scales. The amplitude of

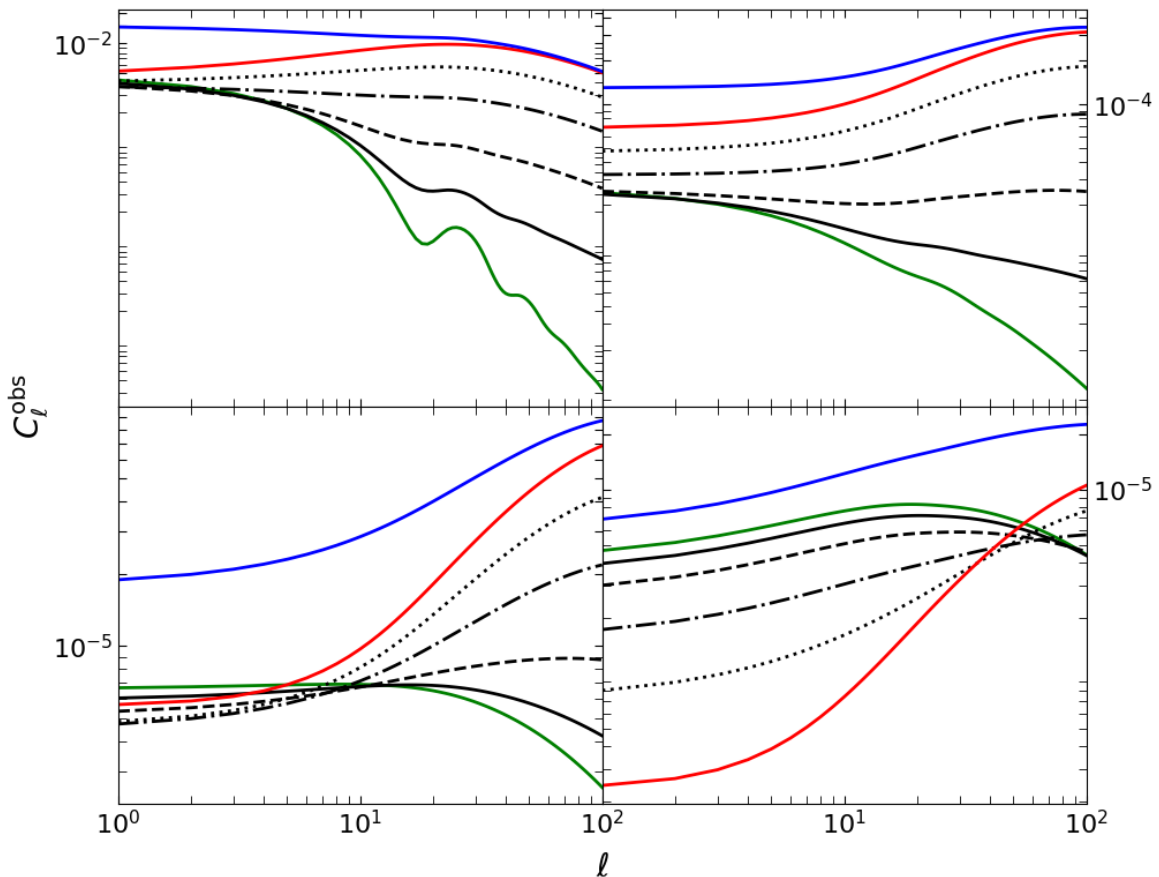


**Figure 2.** The plots of the angular power spectra for magnification bias  $Q=5$ , at the source redshifts:  $z_s = 0.1$  (*top left*),  $z_s = 0.5$  (*top right*),  $z_s = 1$  (*bottom left*) and  $z_s = 3$  (*bottom right*). The line notations are as in Fig. 1. The results for  $Q=-1$  and  $Q=-5$  are identical to those of  $Q=1$  and  $Q=5$ , respectively. Hence those results are not shown in this work.

the total observed angular power spectrum increases as the value of  $\epsilon_v$  increases:  $0 \leq \epsilon_v^2 \leq 1$  with  $\epsilon_{\mathcal{F}}^2 = 1 - \epsilon_v^2$ , as given by (2.11). Note that the observed magnification angular power spectrum corresponds to the total observed angular power spectrum where  $\epsilon_v = 0$  and  $\epsilon_{\mathcal{F}} = 1$  and, conversely, the observed number-count angular power spectrum corresponds to the case where  $\epsilon_v = 1$  and  $\epsilon_{\mathcal{F}} = 0$ . The total observed angular power spectrum with  $\epsilon_v = \epsilon_{\mathcal{F}} = 1$ —which corresponds to previous works—has, as should be expected, higher amplitude on ultra-large scales than the total observed angular power spectrum governed by (2.11). This difference in amplitude increases with increase in redshift, particularly at  $z \geq 1$ . In general, the results show that by computing the magnified and the unmagnified components of the observed, relativistic overdensity and then adding these components directly, the resulting overdensity will lead to an overestimation of the observed angular power spectrum on ultra-large scales. Consequently, this gives a false prediction of the large-scale clustering of galaxies. Moreover, as further shown by the results, the amount by which the large-scale clustering of galaxies is over-projected increases with increasing redshift  $z \geq 1$  (for the given magnification bias  $Q$ ).

In Fig. 2 we illustrate the effect of a large magnification bias. We repeated the computations of Fig. 1, except that here we used the value of magnification bias  $Q=5$ . We see that

most of the features in Fig. 1 are retained in these results. However, we observe reduction in the spread of the lines—and the eventual crossings, at higher redshifts  $z \geq 1$ —for multipoles  $\ell \lesssim 20$ . As already well known, the amplitude of the galaxy power spectrum decreases with increasing redshift, with the contributions of both  $\Delta_n^{\text{obs}}$  and  $\Delta_{\mathcal{M}}^{\text{obs}}$  diminishing accordingly. Moreover, the dominant terms in the (relativistic) observed galaxy overdensity (2.19) come from the observed number-count overdensity (2.16). Note that  $\Delta_{\mathcal{M}}^{\text{obs}}$  changes sign with redshift and multipole: it has negative values at low  $z$  and for large  $\ell$ . On ultra-large scales  $\ell \lesssim 10$ , at redshifts  $z \leq 1$ ,  $\Delta_{\mathcal{M}}^{\text{obs}}$  becomes positive. Thus on these scales, while the contribution of  $\Delta_n^{\text{obs}}$  (which is always positive) decreases with increasing  $z$ ,  $\Delta_{\mathcal{M}}^{\text{obs}}$  is being implicitly multiplied by the same constant value of  $\mathcal{Q} > 1$  (at all  $z$ ), so that as  $\epsilon_{\mathcal{F}}$  increases (where  $\epsilon_{\mathcal{V}}^2 = 1 - \epsilon_{\mathcal{F}}^2$ ), the amplitude of  $\Delta_{\mathcal{M}}^{\text{obs}}$  is gradually boosted; consequently, gradually enhancing the amplitude of the observed angular power spectrum  $C_\ell^{\text{obs}}$  on very large scales. At high redshifts  $z \gtrsim 3$ ,  $\Delta_{\mathcal{M}}^{\text{obs}}$  changes sign relatively earlier, on larger  $\ell \lesssim 60$ . As  $\epsilon_{\mathcal{F}}$  increases ( $\epsilon_{\mathcal{V}}$  decreases),  $\Delta_{\mathcal{M}}^{\text{obs}}$  gives positive contribution in the observed galaxy angular power spectrum; thereby enhancing the amplitude of the observed galaxy angular power spectrum. (Noting that  $\Delta_{\mathcal{M}}^{\text{obs}}$  is the dominant term at the given epochs.)

It should be pointed out that the results for negative values of the magnification bias,  $\mathcal{Q} = -1, -5$ , appear identical to those of the positive values (Figs. 1 and 2), respectively; thus, these results are not shown in this work. Moreover, it is worth noting that when the magnification bias  $\mathcal{Q} = 1$ , there are no any terms in the observed galaxy overdensity (2.19) that will vanish, unlike in the previous works in the literature (corresponding to  $\epsilon_{\mathcal{V}} = \epsilon_{\mathcal{F}} = 1$ ) where the magnification effect cancels almost all volume distortions—as a result, the case where  $\mathcal{Q} = 1$  has been referred to as, e.g. the “diffuse backgrounds” scenario [5] and the “HI intensity mapping” scenario [13]. In this work, the so-called *diffuse backgrounds* or *HI intensity mapping* scenario, will correspond to

$$\epsilon_{\mathcal{V}} = \sqrt{\mathcal{Q}} \epsilon_{\mathcal{F}}, \quad (5.10)$$

where provided the magnification bias is positively valued, the actual value itself is irrelevant: it may or may not be unity—as enforced by previous works. (Obviously, by setting  $\epsilon_{\mathcal{V}} = \epsilon_{\mathcal{F}}$ , we are able to recover the given scenario in previous works, via (5.10)—i.e. if we assume  $\epsilon_{\mathcal{V}} = \epsilon_{\mathcal{F}}$ , then automatically  $\mathcal{Q} = 1$ .) Moreover, by combining (5.10) and (2.11), it implies that for a so-called *diffuse backgrounds* or *HI intensity mapping* scenario, we have  $\epsilon_{\mathcal{V}} = \sqrt{\mathcal{Q}(1 + \mathcal{Q})}^{-1}$  and  $\epsilon_{\mathcal{F}} = \sqrt{(1 + \mathcal{Q})}^{-1}$ , where  $\mathcal{Q}$  is of arbitrary value.

In Fig. 3 we illustrate the effect of the magnification bias  $\mathcal{Q}$  in the observed angular power spectrum  $C_\ell^{\text{obs}}$ . We plot the observed angular power spectrum as a function of the magnification bias for a fixed multipole  $\ell = 10$ , at source redshifts  $z_s = 0.1, 0.5, 1$  and  $3$ . The observed angular power spectrum is computed for various combinations of the values of  $\epsilon_{\mathcal{V}}$  and  $\epsilon_{\mathcal{F}}$ . We see that at low redshifts  $z < 1$ , the amplitude of the observed angular power spectrum grows with increasing magnification bias, for a given set of values of  $\epsilon_{\mathcal{V}}$  and  $\epsilon_{\mathcal{F}}$ . It should be noted that at the given redshifts, magnification effects are insignificant relative to the counts density (of unmagnified, bright sources). We also observe that for a given value of the magnification bias, as  $\epsilon_{\mathcal{V}}$  increases ( $\epsilon_{\mathcal{F}}$  decreases) the amplitude of the observed angular power spectrum also increases, at the given  $z$ —since  $\epsilon_{\mathcal{V}}$  measures the fraction of the unmagnified, intrinsically bright sources in the background distribution density  $\langle \tilde{\mathcal{N}}_g \rangle$ . At the epoch  $z \simeq 1$ , we see a flipping in behaviour of the observed angular power spectrum when the magnification bias  $\mathcal{Q} \simeq 6$ , such that: for  $\mathcal{Q} < 6$ , the observed angular power spectrum grows with increasing  $\epsilon_{\mathcal{V}}$  (decreasing  $\epsilon_{\mathcal{F}}$ ); while for  $\mathcal{Q} \gtrsim 6$ , the observed angular power spectrum

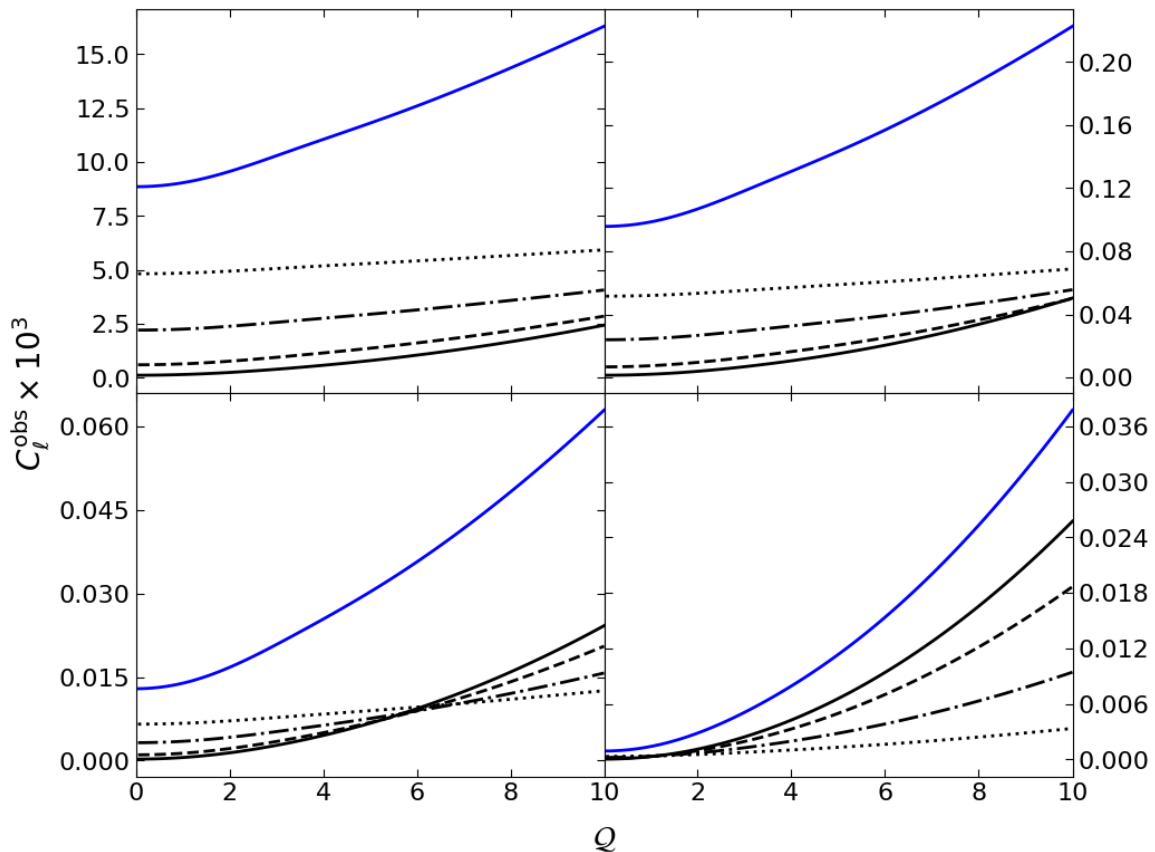


**Figure 3.** The plots of the total angular power spectrum as a function of magnification bias—for multipole  $\ell=10$ , at the source redshifts:  $z_s = 0.1$  (*top left*),  $z_s = 0.5$  (*top right*),  $z_s = 1$  (*bottom left*) and  $z_s = 3$  (*bottom right*). The black lines show the total angular power spectrum for:  $\epsilon_v^2 = 0.1$  and  $\epsilon_F^2 = 0.9$  (solid),  $\epsilon_v^2 = 0.25$  and  $\epsilon_F^2 = 0.75$  (dashed),  $\epsilon_v^2 = 0.5 = \epsilon_F^2$  (dot-dashed) and,  $\epsilon_v^2 = 0.75$  and  $\epsilon_F^2 = 0.25$  (dotted). The blue line shows the result corresponding to previous works ( $\epsilon_v^2 = 1 = \epsilon_F^2$ ).

decreases with increasing  $\epsilon_v$  (decreasing  $\epsilon_F$ ). In other words, the observed angular power spectrum increases with increasing  $\epsilon_F$  (decreasing  $\epsilon_v$ ) for  $Q \gtrsim 6$ , whereas it increases with increasing  $\epsilon_v$  (decreasing  $\epsilon_F$ ) for  $Q < 6$ —at the given redshift. This agrees with the results in Fig. 2 for magnification bias  $Q = 5$ , where we have the observed angular power spectrum changing behaviour: increasing with increasing  $\epsilon_v$  (decreasing  $\epsilon_F$ ), and suddenly decreasing with decreasing  $\epsilon_F$  (increasing  $\epsilon_v$ ), at  $z \simeq 1$ .

At high redshifts  $z > 1$ , the observed angular power spectrum continues to grow with increasing  $\epsilon_F$  (decreasing  $\epsilon_v$ ); however, this growth sets in sooner—from relatively smaller values of the magnification bias  $Q \gtrsim 1$ —unlike at  $z \simeq 1$ , where it only starts growing for  $Q \gtrsim 6$ . This is understandable since magnification effects become substantial and, are the dominant effects, at  $z \gtrsim 3$ . An increasing  $\epsilon_F$  (decreasing  $\epsilon_v$ ) at high redshifts  $z > 1$ , where cosmic magnification becomes significant, results in enhancing the observed angular power spectrum—since  $\epsilon_F$  measures the fraction of the magnified, intrinsically faint sources in the background distribution density. Moreover, we see that throughout the panels in Fig. 3, the result for  $\epsilon_v = 1 = \epsilon_F$  always maintained a relatively higher amplitude for all values of the magnification bias (and  $\epsilon_v < 1$ ,  $\epsilon_F < 1$ ). This implies that the analysis in previous works

will lead to a false overestimation of the clustering strength in structure formation. The results in Fig. 3 essentially suggest that at high redshifts  $z \gtrsim 3$ , sky regions with high cosmic magnification will have strong galaxy clustering, and hence, number of sources. It is also at these same redshifts that relativistic effects are known to be significant. This implies that, a proper understanding of the magnification bias and/or cosmic magnification at these redshifts will be crucial in the analysis of galaxy clustering and relativistic effects.

## 6 Conclusion

A correct, straightforward reanalysis of the relativistic, observed overdensity of cosmological surveys was presented. Along with already known terms, new background parameters  $\epsilon_v$  and  $\epsilon_{\mathcal{F}}$  have been uncovered, and the possible consequence of these parameters in the observed angular power spectrum of galaxies, was demonstrated for the cosmological concordance model.

The new parameters separately quantify: (i) the fraction  $\epsilon_{\mathcal{F}}$  of intrinsically faint background sources, which have been magnified into the observed sample—by the amplification of their flux and/or angular size, and (ii) the fraction  $\epsilon_v$  of the background sources which are intrinsically bright enough to be observed. These parameters dictate the contributions from the magnified (flux-dependent) and the unmagnified (volume-dependent) parts, respectively of the relativistic, observed overdensity; thereby regulating the amplitude of the observed total galaxy power spectrum. Evidently, contrary to previous analyses, the magnified and the unmagnified parts of the relativistic overdensity, in a generic survey, do not merely add; they are scaled by squares of the fractions  $\epsilon_{\mathcal{F}}$  and  $\epsilon_v$ , respectively.

The results showed that, by computing the magnified and the unmagnified components of the observed, relativistic overdensity and then adding these components directly—as done in previous works—the resulting relativistic overdensity will lead to an overestimation of the observed galaxy power spectrum on ultra-large scales. This boost in angular power may lead to false prediction of the large-scale clustering of galaxies. Moreover, as further shown by the results, the amount by which the large-scale clustering of galaxies is over-estimated increases with increasing redshift, particularly at  $z \geq 1$ .

It was also found that the sign (positive or negative) of the magnification bias is not relevant in the large-scale observed galaxy power spectrum. The observed galaxy power spectrum for negative values of the magnification bias  $\mathcal{Q} < 0$ , appear identical to those of the positive values  $\mathcal{Q} > 0$ . Moreover, our calculations ensure that when the magnification bias is unity ( $\mathcal{Q} = 1$ ), there are no any terms in the observed galaxy overdensity that will vanish, unlike in the previous works in the literature—corresponding to  $\epsilon_v = \epsilon_{\mathcal{F}} = 1$ —where the magnification effect cancels almost all volume distortions; as a result, the case where  $\mathcal{Q} = 1$  has been referred to in previous works as the “diffuse backgrounds” scenario [5] and the “HI intensity mapping” scenario [13]. However, in this work the so-called *diffuse backgrounds* or *HI intensity mapping* scenario, will correspond to  $\epsilon_v^2 = \mathcal{Q}(1 + \mathcal{Q})^{-1}$  and  $\epsilon_{\mathcal{F}}^2 = (1 + \mathcal{Q})^{-1}$ .

The results further suggest that at high redshifts  $z \gtrsim 3$ , sky regions with high cosmic magnification will contain strong galaxy clustering, and hence, number of sources. It is also at these same redshifts that relativistic effects are known to be significant. This implies that, a proper understanding of the magnification bias and/or cosmic magnification at these redshifts will be crucial in the analysis of galaxy clustering—and hence, relativistic effects—in the forthcoming surveys.

## Acknowledgements

Thanks to Roy Maartens and Chris Clarkson for meaningful discussions; to Daniele Bertacca for useful comments and, to Bishop Mongwane for assistance with computational facilities. This work was carried out with financial support from (i) the government of Canada’s International Development Research Centre (IDRC), and within the framework of the AIMS Research for Africa Project, and (ii) the South African Square Kilometre Array Project and the South African National Research Foundation.

## A The Number-count and the Magnification Overdensities

In this section we give the explicit forms of the perturbation terms in (2.14), i.e. the density distortion  $\tilde{\delta}_g$ , the volume distortion  $\tilde{\delta}_v$ , and the magnification distortion  $\tilde{\delta}_M$ . (Throughout this work, flat space is assumed—with most of the calculations being drawn from the rigorous work by [6, 12], and relevant references therein.)

### A.1 The metric

We adopt a general metric, given by

$$ds^2 = a(\eta)^2 \left\{ - (1 + 2\phi) d\eta^2 + 2B_{|i} d\eta dx^i + [(1 - 2\psi)\delta_{ij} + 2E_{|ij}] dx^i dx^j \right\},$$

where  $a$  is the scale factor, and  $\eta$  is the conformal time;  $\psi \equiv D + \frac{1}{3}\nabla^2 E$ , and we have used

$$\bar{g}_{00} = -1, \quad \bar{g}_{i0} = \vec{0} = \bar{g}_{0j}, \quad \bar{g}_{ij} = \delta_{ij}, \quad (\text{A.1})$$

and given the 4-scalars  $\phi = \phi(\eta, x^i)$ ,  $B = B(\eta, x^i)$ ,  $D = D(\eta, x^i)$  and  $E = E(\eta, x^i)$ :

$$\delta g_{00} = -2\phi, \quad \delta g_{i0} = B_i, \quad \delta g_{ij} = -2(D\delta_{ij} - E_{ij}), \quad (\text{A.2})$$

where  $B_i = B_{|i}$  and  $E_{ij} = E_{|ij} - \frac{1}{3}\delta_{ij}\nabla^2 E$  is a traceless transverse tensor—i.e.  $E^i_i = 0$ , such that it has no contribution to the term,  $D\delta^i_i$ , in the diagonal plane. (Note that,  $X_{|i} \equiv \nabla_i X$ , and  $X_{|ij} \equiv \nabla_i \nabla_j X$  for a scalar  $X$ .)

The 4-velocities of a particle moving in  $ds$ , are

$$\begin{aligned} u^\mu &= a^{-1} (1 - \phi, v_{|i}), \\ u_\mu &= a (-1 - \phi, v_{|i} + B_{|i}), \end{aligned} \quad (\text{A.3})$$

where  $v$  is the velocity potential (a scalar).

Given (A.1)–(A.3), we define the following potentials

$$\Phi \equiv \phi - \mathcal{H}\sigma - \sigma', \quad (\text{A.4})$$

$$\Psi \equiv D + \frac{1}{3}\nabla^2 E + \mathcal{H}\sigma, \quad (\text{A.5})$$

$$V \equiv v + E', \quad (\text{A.6})$$

which are all gauge-invariant, where  $\sigma = -B + E'$ ;  $\mathcal{H} = a'/a$  is the comoving Hubble parameter, and a prime denotes derivative with respect to conformal time.

## A.2 The density distortion

Here we give the expression for the distortion  $\tilde{\delta}_g$  arising in the galaxy number density  $\tilde{n}_g$ . In order to compute  $\tilde{\delta}_g(\mathbf{n}, z)$ , which is in redshift space, we need to relate it to the distortion  $\delta_g(\mathbf{x}, \eta)$  in real space  $\mathbf{x}$ . Thus by taking a gauge transformation from real to redshift space:

$$\tilde{\delta}_g(\mathbf{n}, z) = \delta_g(\mathbf{n}, z) - \frac{d \ln \bar{n}_g}{d\bar{z}} \delta z(\mathbf{n}, z), \quad (\text{A.7})$$

where the background number density  $\bar{n}_g$  remains the same in both real and redshift spaces, respectively. We have used that, to first order,  $\delta\eta = (\partial\bar{\eta}/\partial\bar{z})\delta z$ . We have

$$\frac{d}{d\bar{z}} \ln \bar{n}_g(\bar{z}) = \frac{3 - b_e(\bar{z})}{1 + \bar{z}}, \quad (\text{A.8})$$

where we used  $a = (1 + \bar{z})^{-1}$ , and the linear galaxy *evolution bias* [5, 6] is given by

$$b_e \equiv \frac{\partial \ln(a^3 \bar{n}_g)}{\partial \ln(a)}, \quad (\text{A.9})$$

with  $a^3 \bar{n}_g$  being the background *comoving* galaxy number per unit volume. Obviously,  $b_e$  measures the *change in the comoving galaxy number density for a given change in redshift*; noting that  $n_g$  measures the *change in galaxy number for a unit change in volume*.

Thus, for volume-limited samples (Sec. 4.3), where there is no change in volume and/or redshift, the galaxy number remains unchanged. Consequently, the background number per unit volume  $\bar{n}_g$  is a *constant*; given (A.8) or (A.9), the evolution bias becomes a constant.

A photon which propagates along the direction  $\mathbf{n}$  from a source  $S$  will be seen by an observer  $O$ , located elsewhere in the universe with fundamental 4-velocity  $u^\mu$ , to be moving with an energy  $\check{E} = -n^\mu u_\mu$  under the direction  $-\mathbf{n}$ . The redshift  $z$  of the propagating photon, in moving from  $S$  to  $O$  is given by (see [3, 6] for details)

$$1 + z = (1 + \bar{z}) \left[ 1 + (\Phi + \Psi + \mathbf{n} \cdot \mathbf{V} - \psi) \Big|_{\bar{z}_S}^0 - \int_{\bar{r}_S}^0 d\bar{r} (\Phi' + \Psi') \right], \quad (\text{A.10})$$

where  $\bar{r}_S = \bar{r}(\bar{z}_S)$  is the background comoving distance<sup>3</sup> at  $S$  (noting that  $\bar{z} = \bar{z}_S$ ),  $\psi$  is a scalar metric potential, and  $\mathbf{V} = \partial_i V$ . The parameters  $\Phi$ ,  $\Psi$  and  $V$  are given by (A.4)–(A.6). A prime (henceforth) denotes derivative with respect to conformal time  $\eta$ . Hence given (A.8) and (A.10), the density distortion (A.7) becomes

$$\begin{aligned} \tilde{\delta}_g(\mathbf{n}, z) &= \Delta_\psi(\mathbf{n}, z) + 3(\Phi + \Psi)(\mathbf{n}, z) + 3\mathbf{n} \cdot \mathbf{V}(\mathbf{n}, z) + 3 \int_{\bar{r}_S}^0 d\bar{r} (\Phi' + \Psi')(\mathbf{n}, \bar{r}) \\ &\quad - b_e(\bar{z}) \left[ \Phi(\mathbf{n}, z) + \mathbf{n} \cdot \mathbf{V}(\mathbf{n}, z) + \int_{\bar{r}_S}^0 d\bar{r} (\Phi' + \Psi')(\mathbf{n}, \bar{r}) \right], \end{aligned} \quad (\text{A.11})$$

where  $\Delta_\psi \equiv \delta_g - 3\psi - b_e \mathcal{H}\sigma$  is the overdensity in flat slicing; terms outside integrals are the relative values between  $S$  and  $O$ . (Note that the  $b_e$  term in (A.11) has been missed by [3, 11].) Thus, we obtain

$$\Delta_\psi = \Delta_g + (3 - b_e) \mathcal{H}V - 3\Psi, \quad (\text{A.12})$$

<sup>3</sup>Note that throughout the appendices,  $r$  denotes the comoving distance, and  $\check{r}$ —given in Secs. 2 and 4—is the (observed) physical distance: along the radial coordinate, or line of sight.

where  $\Delta_g \equiv \delta_g + \bar{n}'_g(v+B)/\bar{n}_g$  is the galaxy comoving overdensity. The galaxy and the matter comoving overdensities, respectively, are related by  $\Delta_g = b\Delta_m$  (see e.g. [6] for a derivation), where  $b$  is the linear *galaxy bias* [5, 6, 15, 16]. The (Gaussian) galaxy bias relates to the evolution bias (A.9), given by [6]

$$b = -\mathcal{H}(3 - b_e) \frac{\bar{\rho}'_m}{\bar{\rho}_m} = 1 - \frac{1}{3}b_e, \quad (\text{A.13})$$

where the second equality follows from the standard continuity equation  $\bar{\rho}'_m = -3\mathcal{H}\bar{\rho}_m$ .

### A.3 The volume distortion

The distortion that arises in the observed volume of galaxy redshift surveys, i.e. the volume density contrast  $\tilde{\delta}_v$ , is given by (see [3, 6, 12] for details)

$$\begin{aligned} \tilde{\delta}_v = & \left( \frac{\mathcal{H}'}{\mathcal{H}^2} + \frac{2}{\bar{r}_s \mathcal{H}} \right) \left[ \Phi + \mathbf{n} \cdot \mathbf{V} - \int_0^{\bar{r}^s} d\bar{r} (\Phi' + \Psi') \right] + \frac{1}{\mathcal{H}} \left[ \Psi' + \partial_r \Phi - \frac{d}{d\lambda} \mathbf{n} \cdot \mathbf{V} \right] - 2(\Phi + \Psi) \\ & - 4\mathbf{n} \cdot \mathbf{V} + 3 \int_0^{\bar{r}^s} d\bar{r} (\Phi' + \Psi') + \int_0^{\bar{r}^s} d\bar{r} \left[ \frac{2}{\bar{r}_s} + (\bar{r} - \bar{r}_s) \frac{\bar{r}}{\bar{r}_s} \nabla_\perp^2 \right] (\Phi + \Psi), \end{aligned} \quad (\text{A.14})$$

where the squared gradient  $\nabla_\perp^2 = \nabla^2 - \partial_r^2 - 2\bar{r}^{-1}\partial_r$  (with  $\partial_r = -\bar{n}^i \partial_i$ ) is the Laplacian on the surface transverse to the line of sight, and  $\lambda$  is an affine parameter along the photon trajectory:  $dX/d\lambda = X' - \partial_r X$ ;  $X$  is a scalar.

By using that galaxies (hence, pressureless matter) move along geodesics, we have the Euler equation for the line-of-sight velocity as

$$\mathbf{n} \cdot \mathbf{V}' + \mathcal{H} \mathbf{n} \cdot \mathbf{V} - \partial_r \Phi = 0. \quad (\text{A.15})$$

Thus given (A.11), (A.12), (A.14) and (A.15), the (observed) number-count overdensity is [6]

$$\begin{aligned} \Delta_n^{\text{obs}}(\mathbf{n}, z) = & \Delta_g(\mathbf{n}, z) - \frac{1}{\mathcal{H}} \partial_r V_{\parallel}(\mathbf{n}, z) + \int_0^{\bar{r}^s} d\bar{r} (\bar{r} - \bar{r}_s) \frac{\bar{r}}{\bar{r}_s} \nabla_\perp^2 (\Phi + \Psi)(\mathbf{n}, \bar{r}) \\ & + (3 - b_e) \mathcal{H} V(\mathbf{n}, z) + \frac{1}{\mathcal{H}} \Psi'(\mathbf{n}, z) - \left( b_e - 1 - \frac{\mathcal{H}'}{\mathcal{H}^2} - \frac{2}{\bar{r}_s \mathcal{H}} \right) \Phi(\mathbf{n}, z) \\ & + \left( b_e - \frac{\mathcal{H}'}{\mathcal{H}^2} - \frac{2}{\bar{r}_s \mathcal{H}} \right) \left\{ V_{\parallel}(\mathbf{n}, z) + \int_0^{\bar{r}^s} d\bar{r} (\Phi' + \Psi')(\mathbf{n}, \bar{r}) \right\} \\ & - 2\Psi(\mathbf{n}, z) + \frac{2}{\bar{r}_s} \int_0^{\bar{r}^s} d\bar{r} (\Phi + \Psi)(\mathbf{n}, \bar{r}), \end{aligned} \quad (\text{A.16})$$

where  $\bar{r}$ ,  $b_e$  and  $\mathcal{H}$  are functions of  $\bar{z}$ ; with  $V_{\parallel} \equiv -\mathbf{n} \cdot \mathbf{V} = \partial_r V$  being the line-of-sight component of the velocity  $\mathbf{V}$ , as seen by  $O$ . The first two lines give the “standard” term of the relativistic number-count overdensity: consisting of the comoving galaxy overdensity, the (Kaiser) redshift distortion term and the weak (gravitational) lensing term, respectively. The standard term constitutes the most dominant contributions (especially at low  $z$ ). The rest of the lines together constitute the “relativistic corrections”; with the third, fourth and fifth lines giving the (peculiar velocity and gravitational) potential effect and the time delay [31] (integral term) in the photon signals. In the last two lines, the first and the second terms in the square brackets correspond to the Doppler and the integrated Sachs-Wolfe (ISW) effects, respectively.

#### A.4 The magnification distortion

Similarly, a lengthy but straightforward calculation (see [5, 6, 12] for details) yields the magnification distortion  $\tilde{\delta}_{\mathcal{M}}$ ; hence the (observed) relativistic magnification overdensity becomes

$$\begin{aligned} \Delta_{\mathcal{M}}^{\text{obs}}(\mathbf{n}, z) = & 2\mathcal{Q}(\bar{z})\Psi(\mathbf{n}, z) - \mathcal{Q}(\bar{z}) \int_0^{\bar{r}_s} d\bar{r} \left[ \frac{2}{\bar{r}_s} - (\bar{r}_s - \bar{r}) \frac{\bar{r}}{\bar{r}_s} \nabla_{\perp}^2 \right] (\Phi + \Psi)(\mathbf{n}, \bar{r}) \\ & + 2\mathcal{Q}(\bar{z}) \left( 1 - \frac{1}{\bar{r}_s \mathcal{H}} \right) \left\{ \Phi(\mathbf{n}, z) - V_{\parallel}(\mathbf{n}, z) - \int_0^{\bar{r}_s} d\bar{r} (\Phi' + \Psi')(\mathbf{n}, \bar{r}) \right\}, \end{aligned} \quad (\text{A.17})$$

where the first line gives the weak lensing term, and the remaining lines give the relativistic effects. Thus, by combining (A.16) and (A.17) we get the explicit form of the (observed) relativistic galaxy overdensity (2.19)—taking note of (2.11).

In general, note that the overdensity  $\Delta_{\mathcal{M}}^{\text{obs}}$  solely measures the “magnification of sources” owing mainly to the magnification of the sources’ fluxes by (A.17): weak lensing, Doppler effect, ISW effect, time delay and (gravitational) potential difference (see [12] for concise statements on these effects, pertaining the magnification of sources). Similarly, the redshift distortions, weak lensing, Doppler effect, ISW effect, time delay and potential difference effects also combine to induce distortions  $\tilde{\delta}_{\nu}$  in the survey volume (see (A.14))—which then increases (or decreases) the number of counted sources—resulting in the “(de)amplification of the number-count overdensity”  $\Delta_n^{\text{obs}}$ . Moreover, notice that there are still some residual lensing/magnification effects left in  $\Delta_n^{\text{obs}}$ ; however, these effects are mainly owing to the inherent volume distortion  $\tilde{\delta}_{\nu}$ , and not owing to dependence on flux/luminosity.

#### References

- [1] J. Yoo, A. L. Fitzpatrick and M. Zaldarriaga, *A New Perspective on Galaxy Clustering as a Cosmological Probe: General Relativistic Effects*, *Phys. Rev. D* **80**, 083514 (2009) [[arXiv:0907.0707](#)].
- [2] J. Yoo, *General Relativistic Description of the Observed Galaxy Power Spectrum: Do We Understand What We Measure?*, *Phys. Rev. D* **82**, 083508 (2010) [[arXiv:1009.3021](#)].
- [3] C. Bonvin and R. Durrer, *What galaxy surveys really measure*, *Phys. Rev. D* **84**, 063505 (2011) [[arXiv:1105.5280](#)].
- [4] A. Challinor and A. Lewis, *The linear power spectrum of observed source number counts*, *Phys. Rev. D* **84**, 043516 (2011) [[arXiv:1105.5292](#)].
- [5] D. Jeong, F. Schmidt and C. M. Hirata, *Large-scale clustering of galaxies in general relativity*, *Phys. Rev. D* **85**, (2012) 023504 [[arXiv:1107.5427](#)].
- [6] D. Duniya, *Relativistic Corrections to the Power Spectrum*, **Ph.D. thesis**, University of the Western Cape, South Africa (2015).
- [7] C. Bonvin, *Isolating relativistic effects in large-scale structure*, *Class. Quant. Grav.* **31**, 234002 (2014) [[arXiv:1409.2224](#)].
- [8] L. Lopez-Honorez, O. Mena and S. Rigolin, *Biases on cosmological parameters by general relativity effects*, *Phys. Rev. D* **85**, 023511 (2012) [[arXiv:1109.5117](#)].
- [9] D. Alonso, P. Bull, P. G. Ferreira, R. Maartens and M. Santos, *Ultra large-scale cosmology in next-generation experiments with single tracers*, *Astrophys. J.* **814**, 145 (2015) [[arXiv:1505.07596](#)].

- [10] J. Renk, M. Zumalacarregui and F. Montanari, *Gravity at the horizon: on relativistic effects, CMB-LSS correlations and ultra-large scales in Horndeski's theory*, *JCAP* **1607**, 040 (2016) [[arXiv:1604.03487](#)].
- [11] R. Durrer and V. Tansella, *Vector perturbations of galaxy number counts*, *JCAP* **1607**, 037 (2016) [[arXiv:1605.05974](#)].
- [12] D. Duniya, *Large-scale imprint of relativistic effects in the cosmic magnification*, *Phys. Rev. D* **93**, 103538 (2016) [[arXiv:1604.03934](#)].
- [13] D. Duniya, D. Bertacca and R. Maartens, *Clustering of quintessence on horizon scales and its imprint on HI intensity mapping*, *JCAP* **1310**, 015 (2013) [[arXiv:1305.4509](#)].
- [14] F. Montanari and R. Durrer, *Measuring the lensing potential with tomographic galaxy number counts*, *JCAP* **1510**, 070 (2015) [[arXiv:1506.01369](#)].
- [15] N. Bartolo, S. Matarrese and A. Riotto, *Relativistic effects and primordial non-Gaussianity in the galaxy bias*, *JCAP* **1104**, 011 (2011) [[arXiv:1011.4374](#)].
- [16] T. Baldauf, U. Seljak, L. Senatore and M. Zaldarriaga, *Galaxy Bias and non-Linear Structure Formation in General Relativity*, *JCAP* **1110**, 031 (2011) [[arXiv:1106.5507](#)].
- [17] J. Yoo, N. Hamaus, U. Seljak and M. Zaldarriaga, *Testing General Relativity on Horizon Scales and the Primordial non-Gaussianity*, *Phys. Rev. D* **86**, 063514 (2012) [[arXiv:1109.0998](#)].
- [18] F. Schmidt and D. Jeong, *Cosmic Rulers*, *Phys. Rev. D* **86**, 083527 (2012) [[arXiv:1204.3625](#)].
- [19] D. Jeong and F. Schmidt, *Large-Scale Structure with Gravitational Waves I: Galaxy Clustering*, *Phys. Rev. D* **86**, 083512 (2012) [[arXiv:1205.1512](#)].
- [20] F. Schmidt and D. Jeong, *Large-Scale Structure with Gravitational Waves II: Shear*, *Phys. Rev. D* **86**, 083513 (2012) [[arXiv:1205.1514](#)].
- [21] D. Bertacca, R. Maartens, A. Raccanelli and C. Clarkson, *Beyond the plane-parallel and Newtonian approach: Wide-angle redshift distortions and convergence in general relativity*, *JCAP* **1210**, 025 (2012) [[arXiv:1205.5221](#)].
- [22] R. Maartens, G. B. Zhao, D. Bacon, K. Koyama and A. Raccanelli, *Relativistic corrections and non-Gaussianity in radio continuum surveys*, *JCAP* **1302**, 044 (2013) [[arXiv:1206.0732](#)].
- [23] S. F. Flender and D. J. Schwarz, *Newtonian versus relativistic cosmology*, *Phys. Rev. D* **86**, 063527 (2012) [[arXiv:1207.2035](#)].
- [24] A. Hall, C. Bonvin and A. Challinor, *Testing General Relativity with 21 cm intensity mapping*, *Phys. Rev. D* **6**, 2013 (87) [[arXiv:1212.0728](#)].
- [25] L. Lombriser, J. Yoo and K. Koyama, *Relativistic effects in galaxy clustering in a parametrized post-Friedmann universe*, *Phys. Rev. D* **87**, 104019 (2013) [[arXiv:1301.3132](#)].
- [26] J. Yoo and V. Desjacques, *All-Sky Analysis of the General Relativistic Galaxy Power Spectrum*, *Phys. Rev. D* **88**, 023502 (2013) [[arXiv:1301.4501](#)].
- [27] D. Jeong and F. Schmidt, *Cosmic Clocks*, *Phys. Rev. D* **89**, 043519 (2014) [[arXiv:1305.1299](#)].
- [28] A. Raccanelli, D. Bertacca, O. Dore and R. Maartens, *Large-scale 3D galaxy correlation function*, *JCAP* **1408**, 022 (2014) [[arXiv:1306.6646](#)].
- [29] E. Di Dio, F. Montanari, J. Lesgourgues and R. Durrer, *The CLASSgal code for Relativistic Cosmological Large Scale Structure*, *JCAP* **1311**, 044 (2013) [[arXiv:1307.1459](#)].
- [30] C. Bonvin, L. Hui and E. Gaztanaga, *Asymmetric galaxy correlation functions*, *Phys. Rev. D* **89**, 083535 (2014) [[arXiv:1309.1321](#)].
- [31] A. Raccanelli, D. Bertacca, R. Maartens, C. Clarkson and O. Dore, *Lensing and time-delay contributions to galaxy correlations*, [arXiv:1311.6813](#).

- [32] D. J. Bacon, S. Andrianomena, C. Clarkson, K. Bolejko and R. Maartens, *Cosmology with Doppler Lensing*, *Mon. Not. Roy. Astron. Soc.* **443**, 1900 (2014) [[arXiv:1401.3694](#)].
- [33] D. Jeong and F. Schmidt, *Large-Scale Structure Observables in General Relativity*, *Class. Quant. Grav.* **32**, 044001 (2015) [[arXiv:1407.7979](#)].
- [34] E. Villa, L. Verde and S. Matarrese, *General relativistic corrections and non-Gaussianity in large scale structure*, *Class. Quant. Grav.* **31**, 234005 (2014) [[arXiv:1409.4738](#)].
- [35] J. Yoo, *Relativistic Effect in Galaxy Clustering*, *Class. Quant. Grav.* **31**, (2014) 234001 [[arXiv:1409.3223](#)].
- [36] S. Camera, M. G. Santos and R. Maartens, *Probing primordial non-Gaussianity with SKA galaxy redshift surveys: a fully relativistic analysis*, *Mon. Not. Roy. Astron. Soc.* **448**, 1035 (2015) [[arXiv:1409.8286](#)].
- [37] S. Camera, R. Maartens and M. G. Santos, *Einstein's legacy in galaxy surveys*, *Mon. Not. Roy. Astron. Soc.* **451**, L80 (2015) [[arXiv:1412.4781](#)].
- [38] D. Duniya, D. Bertacca and R. Maartens, *Probing the imprint of interacting dark energy on very large scales*, *Phys. Rev. D* **91**, 063530 (2015) [[arXiv:1502.06424](#)].
- [39] A. Kehagias, A. M. Dizgah, J. Norena, H. Perrier and A. Riotto, *A Consistency Relation for the Observed Galaxy Bispectrum and the Local non-Gaussianity from Relativistic Corrections*, *JCAP* **1508**, 018 (2015) [[arXiv:1503.04467](#)].
- [40] D. Duniya, *Dark energy homogeneity in general relativity: Are we applying it correctly?*, *Gen. Rel. Grav.* **48**, 52 (2016) [[arXiv:1505.03436](#)].
- [41] A. Raccanelli, F. Montanari, D. Bertacca, O. Dore and R. Durrer, *Cosmological Measurements with General Relativistic Galaxy Correlations*, [arXiv:1505.06179](#).
- [42] N. Bartolo *et al.*, *A relativistic signature in large-scale structure*, *Phys. Dark Univ.* **13**, 30 (2016) [[arXiv:1506.00915](#)].
- [43] D. Alonso and P. G. Ferreira, *Constraining ultralarge-scale cosmology with multiple tracers in optical and radio surveys*, *Phys. Rev. D* **92**, 063525 (2015) [[arXiv:1507.03550](#)].
- [44] J. Yoo and J. O. Gong, *Relativistic effects and primordial non-Gaussianity in the matter density fluctuation*, *Phys. Lett. B* **754**, 94 (2016) [[arXiv:1509.08466](#)].
- [45] V. Irsic, E. Di Dio and M. Viel, *Relativistic effects in Lyman- $\alpha$  forest*, *JCAP* **1602**, 051 (2016) [[arXiv:1510.03436](#)].
- [46] E. Di Dio, R. Durrer, G. Marozzi and F. Montanari, *The bispectrum of relativistic galaxy number counts*, *JCAP* **1601**, 016 (2016) [[arXiv:1510.04202](#)].
- [47] C. Bonvin, L. Hui and E. Gaztanaga, *Optimising the measurement of relativistic distortions in large-scale structure*, [arXiv:1512.03566](#).
- [48] E. Gaztanaga, C. Bonvin and L. Hui, *Measurement of the dipole in the cross-correlation function of galaxies*, [arXiv:1512.03918](#).
- [49] A. Raccanelli, D. Bertacca, D. Jeong, M. C. Neyrinck and A. S. Szalay, *Doppler term in the galaxy two-point correlation function: wide-angle, velocity, Doppler lensing and cosmic acceleration effects*, [arXiv:1602.03186](#).
- [50] D. Duniya, T. Moloi, C. Clarkson, J. Larena, R. Maartens, B. Mongwane and A. Weltman, *Probing beyond-Horndeski gravity on ultra-large scales*, [arXiv:1902.09919](#).
- [51] F. D. Albareti *et al.* [SDSS Collaboration], *The 13th Data Release of the Sloan Digital Sky Survey: First Spectroscopic Data from the SDSS-IV Survey Mapping Nearby Galaxies at Apache Point Observatory*, *Astrophys. J. Suppl.* **233**, no. 2, 25 (2017) [[arXiv:1608.02013](#)].

- [52] S. A. Shectman, S. D. Landy, A. Oemler, D. L. Tucker, H. Lin, R. P. Kirshner and P. L. Schechter, *The Las Campanas Redshift Survey*, *Astrophys. J.* **470**, 172 (1996) [[astro-ph/9604167](#)].
- [53] H. Lin, R. P. Kirshner, S. A. Shectman, S. D. Landy, A. Oemler, D. L. Tucker and P. L. Schechter, *The power spectrum of galaxy clustering in the las campanas redshift survey*, *Astrophys. J.* **471**, 617 (1996) [[astro-ph/9606055](#)].
- [54] R. Ziour and L. Hui, *Magnification Bias Corrections to Galaxy-Lensing Cross-Correlations*, *Phys. Rev. D* **78**, 123517 (2008) [[arXiv:0809.3101](#)].
- [55] F. Schmidt, E. Rozo, S. Dodelson, L. Hui and E. Sheldon, *Size Bias in Galaxy Surveys*, *Phys. Rev. Lett.* **103**, 051301 (2009) [[arXiv:0904.4702](#)].
- [56] F. Schmidt and E. Rozo, *Weak Lensing Peak Finding: Estimators, Filters, and Biases*, *Astrophys. J.* **735**, 119 (2011) [[arXiv:1009.0757](#)].
- [57] J. Liu, Z. Haiman, L. Hui, J. M. Kratochvil and M. May, *The Impact of Magnification and Size Bias on Weak Lensing Power Spectrum and Peak Statistics*, *Phys. Rev. D* **89**, 023515 (2014) [[arXiv:1310.7517](#)].
- [58] S. Camera, C. Fedeli and L. Moscardini, *Magnification bias as a novel probe for primordial magnetic fields*, *JCAP* **1403**, 027 (2014) [[arXiv:1311.6383](#)].
- [59] H. Hildebrandt, *Observational biases in flux magnification measurements*, *Mon. Not. Roy. Astron. Soc.* **455**, 3943 (2016) [[arXiv:1511.01352](#)].
- [60] A. F. Heavens and B. Joachimi, *Cosmic magnification: nulling the intrinsic clustering signal*, *Mon. Not. Roy. Astron. Soc.* **415**, 1681 (2011) [[arXiv:1101.3337](#)].
- [61] B. Gillis and A. Taylor, *A Generalized Method for Measuring Weak Lensing Magnification With Weighted Number Counts*, *Mon. Not. Roy. Astron. Soc.* **456**, 2518 (2016) [[arXiv:1507.01858](#)].
- [62] V. J. Martinez and E. Saar, *Statistics of the Galaxy Distribution*, Chapman & Hall/CRC (2002).
- [63] M. LoVerde and N. Afshordi, *Extended Limber Approximation*, *Phys. Rev. D* **78**, 123506 (2008) [[arXiv:0809.5112](#)].
- [64] S. Dodelson, *Modern Cosmology*, Academic Press (2003).